PRAMANA — journal of physics

Vol. 84, No. 6
June 2015
pp. 1073–1086

High-capacity electrode materials for electrochemical energy storage: Role of nanoscale effects

JAGJIT NANDA[1,4,5,*], SURENDRA K MARTHA[2] and RAMKI KALYANARAMAN[3,4,5]

[1]Materials Science & Technology Division, Oak Ridge National Laboratory, Oak Ridge, TN 37831, USA
[2]Department of Chemistry, Indian Institute of Technology Hyderabad, ODF Estate, Yeddumailaram 502 205, India
[3]Materials Science & Engineering Department, The University of Tennessee, Knoxville, TN 37994, USA
[4]Bredesen Center, University of Tennessee, Knoxville, TN, USA
[5]Chemical and Biomolecular Engineering, The University of Tennessee, Knoxville, TN 37994, USA
*Corresponding author. E-mail: nandaj@gmail.com

DOI: 10.1007/s12043-015-1006-8; ***e*Publication:** 2 June 2015

Abstract. This review summarizes the current state-of-the art electrode materials used for high-capacity lithium-ion-based batteries and their significant role towards revolutionizing the electrochemical energy storage landscape in the area of consumer electronics, transportation and grid storage application. We discuss the role of nanoscale effects on the electrochemical performance of high-capacity battery electrode materials. Decrease in the particle size of the primary electrode materials from micron to nanometre size improves the ionic and electronic diffusion rates significantly. Nanometre-thick solid electrolyte (such as lithium phosphorous oxynitride) and oxides (such as Al_2O_3, ZnO, TiO_2 etc.) material coatings also improve the interfacial stability and rate capability of a number of battery chemistries. We elucidate these effects in terms of different high-capacity battery chemistries based on intercalation and conversion mechanism.

Keywords. High capacity; cathode materials; Li-rich NMC; conversion cathodes; lithium-ion battery.

PACS Nos 82.47.Aa; 61.46.−w; 81.07.−b

1. Introduction

Energy storage technologies are central towards the development and wide-scale acceptability of renewable energy sources for reducing greenhouse gas emission. Intermittent sources such as solar and wind energies need reliable and efficient energy storage systems

that can store energy during peak generation and then supply uninterrupted power on demand. During the last decade, rapid advancement has been made in the area of electrochemical energy storage devices such as batteries and supercapacitors [1]. Such progress has been mostly possible due to the development of new electrode materials that can reversibly store more charge per unit volume or weight of the active material. In the area of batteries, the most significant development has been the development of high-capacity positive (cathode) and negative (anode) electrode materials for lithium-ion-based batteries [1]. This has almost revolutionized the battery technology landscape in terms of their volumetric and gravimetric energy densities compared to conventional alkaline cells or even nickel-metal hydride batteries [2]. To provide an example, a typical lithium-ion battery has a nominal voltage of 3.7 V with specific capacity in the range of 150 mAh g^{-1}, in contrast to the advanced nickel-metal hydride batteries which nominally operate at 1.2 V with a specific capacity of about 400 mAh g^{-1} [2]. The chemistry of most of the high-capacity batteries is fundamentally based on a number of redox mechanisms such as intercalation, displacement, or conversion. Among them, the intercalation-based batteries have been successfully commercialized because of their robust reversibility and cycle life. Lithium-ion batteries are classic examples of intercalation-based batteries which was reported early on by Stanley Whittingham and John Goodenough for two different classes of compounds [3,4]. The schematic of the working principle of lithium-ion battery is illustrated in figure 1. The positive electrode commonly referred to as the cathode is the lithium reservoir which generally consists of lithium-based transition metal oxides. The negative electrode referred to as the anode is graphitic carbon. During the charge process, lithium ions diffuse

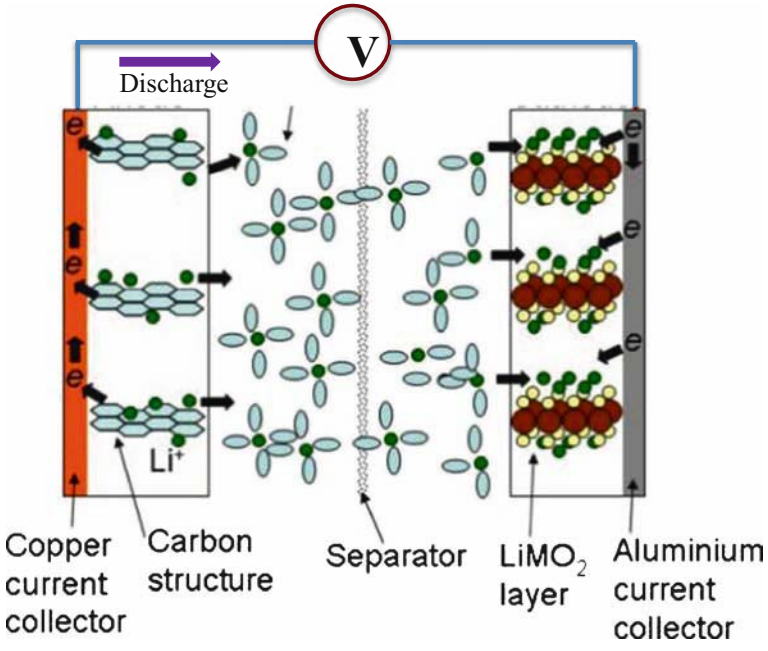

Figure 1. Working principle of lithium-ion cells. For convenience, the operation is only shown for the discharge state (see text).

from the host cathode particles and reach the electrode interface to be transported by the electrolyte to the anode via the porous separator. The electrons travel through the back of the electrode to the current collector and pass through the external circuit to reach the anode. The lithium ions are intercalated in the graphitic layers and gradually get filled up with increasing charging voltage, which is nominally around 4.2 V for standard Li-ion batteries. During the discharge, the lithium ions leave the graphitic layers and get back to the lithium host (as illustrated in figure 1). The electrochemical reaction can be written in a simplified way as

Charge:

$LiMO_2 \rightarrow xLi^+ + xe^- + Li_{1-x}MO_2$, where M = Mn, Ni or Co or a combination of all the three elements (at the cathode).

$xLi^+ + xe^- + 6C \rightarrow LiC_6$ (at the anode).

Discharge:

$xLi^+ + xe^- + Li_{1-x}MO_2 \rightarrow LiMO_2$ (at the cathode).

$LiC_6 \rightarrow xLi^+ + 6C + xe^-$ (at the anode).

The electrolyte for the standard lithium-ion batteries comprises lithium hexafluorophosphate salt ($LiPF_6$) dissolved in a mixture of dimethyl carbonate (DMC) and ethyl carbonate (EC). The separator typically is in the range of 25 micron thickness and consists of a multilayer of polyethylene–polypropylene with pore sizes in the range of tens of nanometres [5]. This article summarizes the material aspects of the current lithium-ion-based batteries and provides an insight on the role of nanosizing the electrode materials for better electrochemical transport and capacity retention. The article is organized as follows: Section 2 provides a brief summary of the current state-of-the-art lithium-ion batteries and the material challenges for achieving higher energy density. Section 3 discusses the need for nanostructuring at a material and interface level for optimizing the electrochemical transport kinetics. Section 4 discusses some examples of specific high capacity cathode chemistries and their performances. Section 5 provides a brief discussion on some high-energy density systems that are beyond the standard lithium intercalation-based chemistries.

2. Two decades of lithium-ion batteries: Current status and research challenges

Lithium-ion battery was first commercialized by Sony in the year 1991 and since then has become a huge success in the area of consumer electronics, power applications, and automobiles. The batteries, since then, have started becoming more robust with high-energy density primarily due to the development and commercialization of electrode materials. Lithium cobalt oxide ($LiCoO_2$)–carbon was the first battery chemistry to be commercialised (by Sony) and since then a number of new high-capacity chemistries have been developed [4]. Examples include lithium iron phosphate ($LiFePO_4$), variations of lithium nickel manganese cobalt oxide (e.g. $LiNi_{0.33}Mn_{0.33}Co_{0.33}O_2$), spinel and high voltage spinel ($LiMn_2O_4$, $LiMn_{1.5}Ni_{0.5}O_4$) [6,7]. To keep up with the increasing market demands for higher energy density, increased cycle life, better safety and lower cost, the

search for new materials with high lithium storage capacity has become the central part of research and development efforts [8]. In terms of the technological barrier, development of high-capacity cathodes for Li ion is the key for increasing the energy density. This is so because carbon, the widely used anode for Li ion, has a specific capacity of 372 mAh g^{-1}, while specific capacities of most of the performing cathodes are in the range of 150–180 mAh g^{-1}, which is only half the capacity of the anode. To address this issue, there has been substantial effort towards finding new high-capacity and/or high-voltage cathode chemistries. The energy density of a specific redox chemistry, to a first approximation, is a product of the nominal voltage of the redox reaction times the specific capacity. Recent developments of high voltage spinel and over-lithiated lithium nickel–manganese–cobalt oxide (NMC) are some examples which will be discussed later in this paper [7,9–14]. For the anode materials we have a number of candidates beyond lithiated graphite which have significantly higher capacities [15–18]. Examples include Si, Sn and mixed alloy compositions such as Cu–Sn(Fe) [19–22]. These materials have significantly higher capacity than carbon. For example, Si has a theoretical capacity close to 4000 mAh g^{-1} [23]. But these anodes, despite their extremely high capacity, have other materials and interfacial challenges which affects their cycle life. These include high volume expansion (contraction) upon lithiation (delithiation) which can be typically around 310% at full lithiation, and an unstable surface electrolyte interface (SEI) layer that is constantly evolving with each new cycle [23]. Due to these reasons, eventhough high capacity anodes are still not commercialized, they will play increasingly larger roles towards the development of higher energy density lithium-ion batteries. Apart from the energy density aspects other important reasons for the mass production of Li-ion batteries are improved safety and lower cost. The last few years have brought to attention a number of safety issues involving fires with Li-ion battery packs due to thermal runaway events [24,25]. Thermal safety is very closely linked with specific electrode chemistry with some compositions being structurally more unstable under charged conditions, resulting in higher oxygen evolution under charging, leading to thermal hazards. When the cathode is fully charged, there is a tendency for the transition metal oxide to release oxygen, which reacts with the organic carbonates in the electrolyte and triggers catastrophic 'thermal runaway'. It was found that, while the cathode chemistry dictates the severity of thermal runaway, electrolytes modified with fluoroalkyl phosphates and phosphazenes could help by raising the onset threshold of thermal reactions [26]. At present, the cost per kilowatt hour for Li-ion batteries are in the range of $300–350. This is still about a factor of three higher, if it is to be competitive with gasoline engine counterparts for automotive applications. The United States Department of Energy (DOE) has a cost projection target of about $125/KW h for the year 2020.

3. Nanoscale effects: Battery electrode materials and interfaces

Ideally, the thermodynamics of the redox system dictates the directionality and the voltage of the electrochemical reaction. The Gibbs energy of a redox system is typically expressed by $\Delta G = -nFE$, where n is the number of electrons involved in the redox process, F is the Faraday number and E is the redox potential (in volts). The energy density (ED) is given by, ED $= E \times Q$, where Q is the specific capacity given by $Q = nF/M_w$, M_w is

the molecular weight [27]. A higher voltage difference between the cathodic and anodic process is crucial for higher energy density. The kinetics aspect deals with the reaction rates, both for bulk electrode material and at the electrode–electrolyte interface. Fast kinetics is important for high power applications. Better electrochemical performance requires optimized mass transport where both ionic and electronic transport is not rate-limited [27]. A good cathode material should have reasonably good intrinsic ionic and electronic conductivities. Nevertheless, making the primary electrode particle size in the nanometre range provides additional benefits due to the reduction in the diffusion length scale for ionic transport. In a simplistic way, the mean ion diffusion time (t_{ion}) can be correlated with the average particle size L by the expression, $t_{\text{ion}} = L^2/D_{\text{ion}}$, where D_{ion} is the ion diffusion coefficient. For a given D_{ion}, reducing the particle size from 100 nm to 10 nm improves the ion diffusion by two orders of magnitude. In most cases, electronic conductivity of an electrode can be increased by a nanoscale carbon coating [28,29] or by adding a few percent of graphitic carbon nanofibre [10]. The next section elucidates the role of nanoscale effects on the electrochemical performance of battery cathode materials.

4. High voltage and capacity lithium-ion cathodes

In early 2000, Thackeray, Johnson *et al* at Argonne National Laboratory [9,11,30] reported lithium–manganese-rich layered–layered structure given by the nominal composition $x\text{Li}_2\text{MnO}_3\cdot(1-x)\text{LiMO}_2$, where M = Mn, Ni and Co which when cycled to voltages >4.5 V provide reversible capacities >250 mAh g^{-1} after the first cycle. The basic premise behind this high capacity can be described in the following steps: (i) till 4.3 V charge the capacity contribution comes from lithium located in the interstitial space between the TM and oxygen layer. (ii) At approximately 4.4–4.5 V, the Li_2MnO_3 component gets activated and subsequently releases two lithium and one oxygen at the surface to form a layered MnO_2-type composition [9–11]. It is feasible that further oxygen loss could occur in the lattice which would destabilize the layered structure at these high voltages. The net removal of Li_2O yields a very high anomalous capacity (320–340 mAh g^{-1}) upon first charging the cycle to 4.8 V. At the end of the first charge (full delithiation), the cathode composition can be described as $x\text{MnO}_2\cdot(1-x)\text{MO}_2$. The oxygen loss [31,32] during the first cycle is irreversible and upon subsequent lithiation (second cycle onwards) this composition can also be described as $x\text{LiMnO}_2\cdot(1-x)\text{LiMO}_2$, with MnO_2 unit only able to uptake one Li atom. Depending on the composition of the parent Li_2MnO_3 phase and TM stoichiometry, this cathode can still provide reversible capacity in the range of 260–270 mAh g^{-1} which is almost a factor of two higher than even the high voltage manganese–nickel spinel ($\text{LiNi}_{0.5}\text{Mn}_{1.5}\text{O}_4$) [10]. Subsequently, this cathode composition was licensed to industrial partners like Toda Kyogo, Envia Systems and BASF for developing high energy density lithium ion cells for plug-in electric vehicles.

LMR–NMC powder was obtained from the pilot scale synthesis facility of Toda Kyogo Ltd., Japan and detailed structural and electrochemical characterization studies were performed at Oak Ridge National Laboratory. Figures 2a and 2b show representative SEM micrographs at various magnifications of pristine LMR–NMC secondary particles having a spherical morphology with an average particle diameter ranging between 5 and

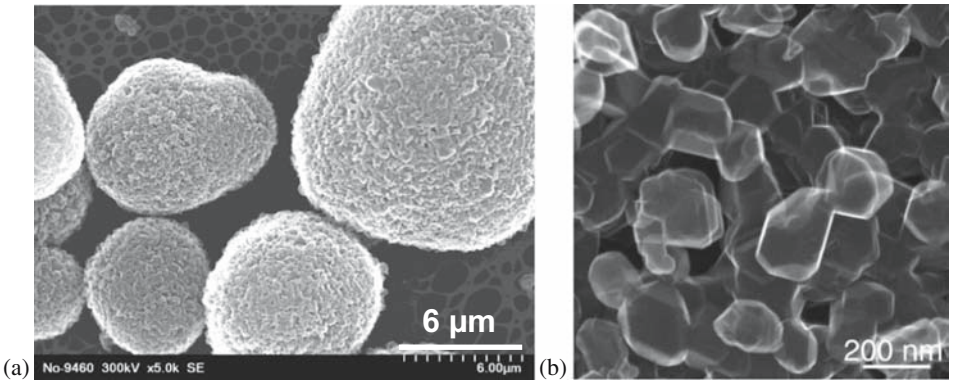

Figure 2. SEM images at various magnifications of the LMR–NMC starting material. (**a**) secondary particles, (**b**) primary particles.

15 μm (figure 2a). Higher magnification images show secondary particles comprising primary particles with faceted surfaces in the size range of 100 nm (figure 2b). The active surface area of the material was estimated to be 3.2 $m^2\ g^{-1}$ by the Brunauer, Emmet and Teller (BET) method with a tap density of about 1.74 g cm^{-3}. Tap density is a measure of compactness of the electrode material. Higher tap density is preferable for increasing the energy density at a volumetric level. Electrodes were prepared with N-methylpyrrolidone (NMP), slurry of Li-rich NMC, polyvinylidene fluoride (PVDF) (Aldrich) and carbon black (CB) (Super P) carbon nanofibre in 1.5 wt% ratio of 85:7.5:6:1.5. The electrodes comprised $\sim$5 mg of active Li-rich NMC per cm^2 on Al and were about 75 μm thick. Lithium foils (purity 99.9%, Alfa Aesar) were used as counter electrodes. The electrolyte solution was 1.2 M $LiPF_6$ in a 1:2 mixture of ethylene carbonate (EC) and dimethyl carbonate (DMC) by weight (battery grade, Novolyte Technologies, USA). The electrochemical performance of the cathodes comprising Li-rich NMC as the active mass was evaluated using two-electrode coin-type cells (size CR2032, Hohsen Corp., Japan) with a 25 μm microporous trilayer membrane (polypropylene/polyethylene/polypropylene) separator (type 2325, Celgard, Inc., USA) in glove boxes (Innovative Technology, Inc., USA) filled with high-purity argon. After assembling, the cells were stored at room temperature for about 12 h to ensure complete impregnation of the electrodes and separators with the electrolyte solution. Galvanostatic charge–discharge cycling was carried out using a multichannel battery tester (model 4000, Maccor Inc., USA) in two-electrode coin-type cells. The cells were discharged galvanostatically at $C/10$ rate, followed by galvanostatic charging at $C/5$ rate to 4.9 V, followed by potentiostatic charge until the current reaches $C/50$. The cells were discharged at a constant current with a cut-off potential at 2.0 V [10].

The electrochemical performance of the composite electrode was carefully investigated at charge–discharge current density similar to $C/10$, and is shown in figure 3. Maximum capacity of 280 mAh g^{-1} (at a cut-off potential of 4.9 V at $C/10$ rate) can be achieved by adding a small fraction of carbon nanofibre (CNF) to LMR–NMC electrodes as demonstrated by us in a previous study. The amount of CNF was between 0.5 and 2 wt% but this helps to maintain stable capacities for hundreds of cycles. When these cells are cycled

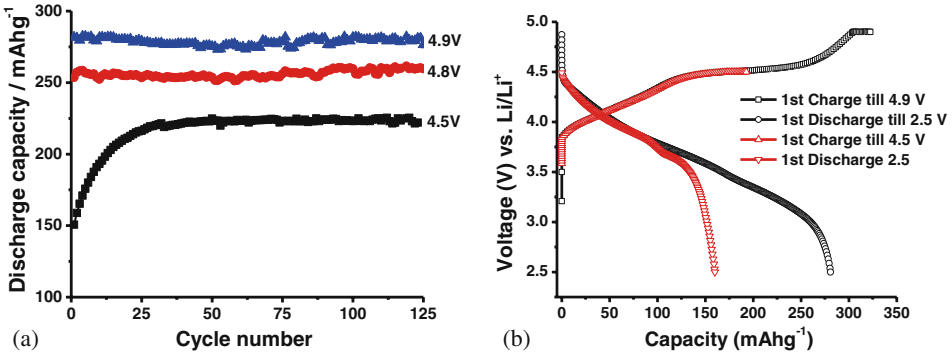

Figure 3. (**a**) Discharge capacity data at various potentials (as indicated) of LMR–NMC composite electrodes at $C/10$ rate, in EC-DMC 1:2/$LiPF_6$ 1.2 M solutions (coin-type cell, $T = 25°C$). Cycling protocol was constant current–constant voltage providing potentiostatic steps at desired higher cut-off potential until the current reaches the value of $C/50$. The lower cut-off potential was 2.5 V vs. Li/Li+. (**b**) Voltage profiles of LMR–NMC composite electrodes measured galvanostatically at $C/10$ rate during the first cycle at 4.9 V cut-off and 4.5 V (12 h potentiostatic hold) at 25°C.

between 2.5 and 4.5 V, an initial capacity of 160 mAh g^{-1} can be achieved. However, with the increase in the number of cycles, the capacity increases, and reversible capacities up to 220 mAh g^{-1} can be achieved for these electrodes within this potential range. As already mentioned in [9–11], Li_2MnO_3 is activated above 4.4 V. The gradual increase in capacity can be attributed to the slow activation of a small amount of Li_2MnO_3 component at 4.5 V. The charge–voltage profiles presented in figure 3b clearly indicates that activation does not complete at 4.5 V. Further charging to 4.8 V and above, results in the almost complete activation of Li_2MnO_3, plausibly forming Li_2O and MnO_2. The detailed mechanism of the activation process is still not understood completely. Increasing the cycling window from 4.8 to 4.9 V results in a 10% increase in capacity for these LMR–NMC composite electrodes. During their operation between 2.5 and 4.9 V, the cells retain 90% of their capacity over 300 cycles and almost 50% capacity for about 600 cycles (0.01% per cycle) with deep discharge as shown in figure 4. Faradaic efficiency close to 99% was observed for these cells during the operation of cells. Conventional LMR–NMC electrodes (no CNF) have limited capacity retention upon prolonged high voltage (4.9 V) cycling, and also exhibit poor rate capability. For the most part this is due to significant reduction in the electronic conductivity because of the formation of insulating electrolyte decomposition and reaction products on the cathode surface which were confirmed by electrochemical impedance spectroscopy and X-ray photoelectron spectroscopy [14]. In contrast, CNFs still provide an effective electronic wiring around the surface of the active material forming an interconnected conducting pathway across the bulk of the electrode despite the formation of a surface passivation film upon high voltage cycling [10].

Apart from improving the electronic conductivity by adding CNFs, the interfacial stability of the high-voltage cathodes can be improved by various nanocoating approaches. Typically, high-voltage cathodes are cycled at voltages >4.5 V. This is above the stable

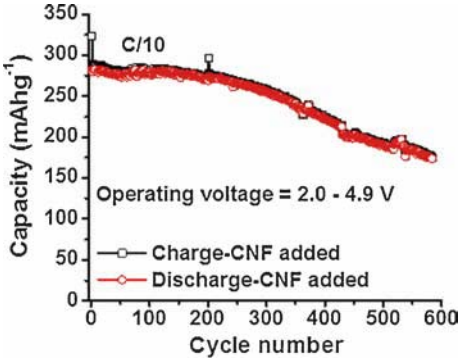

Figure 4. Charge–discharge cycling data at various potentials (as indicated) of LMR–NMC composite electrodes at $C/10$ rate, in EC-DMC 1:2/$LiPF_6$ 1.2 M solutions (coin-type cell, $T = 25°C$). The cycling protocol was the same as described in figure 3.

electrochemical window for most common liquid electrolytes used for LiBs, namely, $LiPF_6$ in a mixture of carbonate solvents (ethylene carbonate and dimethyl carbonate). At higher voltages, the delithiated cathode surfaces are highly oxidized and react with electrolyte to form a decomposition product that can be detrimental to capacity retention and cycle life. To stabilize such interface reactivity, the surface of the cathode particle is coated with inorganic oxides that are conducive to lithium transport. There have been numerous examples in literature in the recent past where nanometre-thick coatings are applied to a range of lithium-ion cathodes and anodes for improving the cycle life and capacity retention. Below, we discuss our recent results wherein a nanometre-thick layer coating of lithium conducting solid electrolyte, lithium phosphorus oxynitride (Lipon), [13,33] is applied on the high-voltage LMR–NMC cathodes. Lipon film was deposited onto active cathode particles as well as on the surface of the electrodes using RF magnetron sputtering technique as described in our earlier publication [13,34]. A comparison of voltage profiles for the conventional, CNF-additive (electronically conducting matrix) and lipon coating (ion conducting matrix-interfacial stability) indicates lipon coating on LMR–NMC have low charge voltage and high discharge voltage indicating lower polarization (figures 5a and 5b). The study showed that a few nm thick (1 h) lipon film is very effective for improving the interfacial stability against high-voltage cycling leading to better cycle life and higher useable capacity [21]. CNF addition further improves the rate performance in comparison to conventional LMR–NMC cathodes (no CNF or lipon coating) as shown in figure 5c. As shown, the lipon-coated Li-rich NMC cathode still has a capacity of >150 mAh g^{-1} at $5C$, ~ 100 mAh g^{-1} at 20°C. On the contrary, the conventional and CNF-added LMR–NMC cathodes show only 60 mAh g^{-1} and 120 mAh g^{-1} capacities at $5C$ discharge rate with no appreciable capacity beyond $5C$. Our results showed that the presence of lipon at the interface significantly improved the C-rate performance. As shown, the rate performance is improved by a factor of 4 or 5 between conventional-CNF added and lipon-coated electrodes at $5C$ and higher rates (figure 5c). Lipon and CNF-added LMR–NMC electrodes demonstrated better Coulombic efficiency compared to conventional electrode.

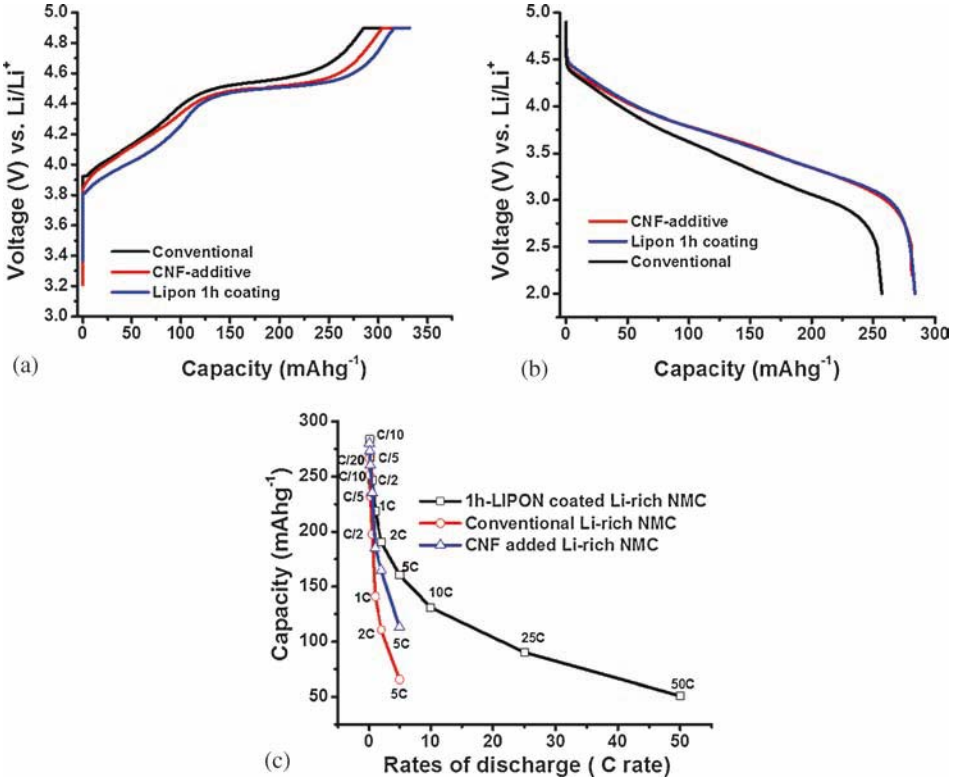

Figure 5. (**a**) Charge and (**b**) discharge voltage profiles of LMR–NMC composite electrodes measured galvanostatically at $C/10$ rate during first cycles at 4.9 V cut-off for conventional, CNF-added and lipon-coated electrodes at 25°C. (**c**) Comparison of rate capabilities (discharge capacity vs. rates) for conventional and CNF added and lipon coated on to LMR–NMC particle composite electrodes measured galvanostatically at various rates (as indicated) at 25°C.

4.1 *Hysteresis and structural transition (voltage fade) in LMR–NMC*

During prolonged cycling, CNF-added electrodes have better cycle life than the lipon-coated electrode over continuous high voltage cycling (2.0–4.9 V). The CNF improves the surface electronic conductivity of the Li-rich NMC particles, and further, provides a conducting path for electrons to reach the current collector across the electrode thickness. CNF-added electrodes retain over 97% capacity after 200 cycles (figure 6a). Interestingly, even after 590 cycles the cells retain a capacity of over 63% (figure 4). While addition of CNF improves the rate performance (figure 5c) and cycle life (figure 6a) to some degree, it cannot address issues related to the interfacial and surface reactions resulting in electrolyte decomposition throughout the high voltage cycling.

Electrochemical measurements on lithium half cells using LMR–NMC electrodes show that the discharge profiles (figure 6b) move to lower voltage plateaus, showing significant voltage fade or suppression of the discharge profile gradually moving to a plateau

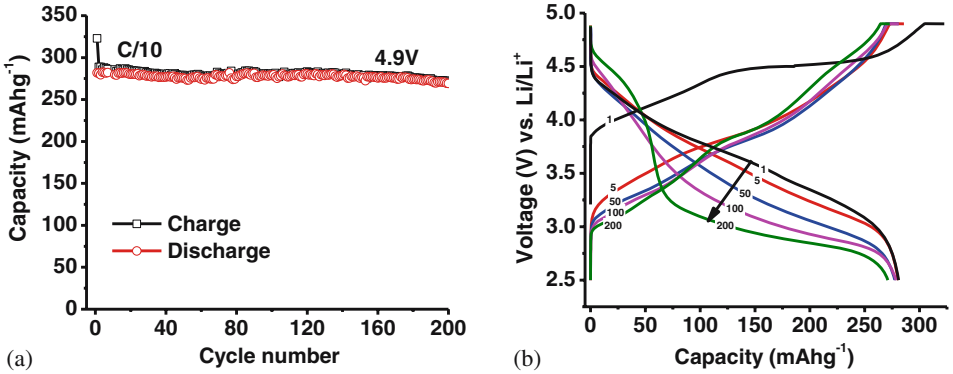

Figure 6. **(a)** Charge–discharge cycling of LMR–NMC composite electrodes measured galvanostatically at $C/10$ rate and 4.9 V cut-off for CNF-added electrodes at 25°C. **(b)** Voltage profiles of CNF-added LMR–NMC composite electrodes measured galvanostatically at $C/10$ rate during 200 cycles (cycle numbers are indicated in the voltage profiles) at 25°C. The cycling protocol was the same as above.

below 3 V when cycled >200 times. Similar behaviour was also noticed for lipon-coated electrodes when cycled over continuous high voltage cycling (2.0–4.9 V) [10,13]. This provides clear experimental evidence that surface coating can improve the interfacial stability and capacity utilization at higher C-rates but it cannot prevent the changes in the bulk material phase during electrochemical cycling.

The discharge profiles gradually change to a lower voltage with a clear plateau developing around 3 V, which typically corresponds to a spinel profile [12,35]. This provides electrochemical evidence that the structure of the cathode materials is possibly changing with high voltage cycling, which has been confirmed extensively by electron microscopy. Overall, although LMR–NMC cathode is promising in terms of high capacity, there still remain significant challenges in terms of structural stability and transition metal dissolution [10,13].

4.2 *High capacity conversion cathodes: Nanoiron fluorides and oxides*

So far we have discussed battery chemistries that show high reversible capacity based on intercalation. Intercalation reactions are generally topotactic with no significant changes in structure during ion transfer. There are other redox mechanisms that demonstrate at least a factor of 3–5 higher capacity than the conventional lithium-ion materials [36,37] but this increase in capacity comes with significant phase change and/or structural instability of the electrode material. Examples include conversion type compounds where nanosizing is important for retaining electrochemical capacity and cycle life.

Recently, multivalent conversion-based binary and ternary compounds have been a subject of particular interest because of their high specific capacity originating from multiple oxidation states over a relatively large voltage window [37–40]. Typically, the binary phase conversion reactions proceed via, $n\mathrm{Li}^+ + n\mathrm{e}^- + \mathrm{Me}^{n+}\mathrm{X} \leftrightarrow \mathrm{LiX} + \mathrm{Me}^0$ where Me is a transition metal element and X belong to an oxide, sulphide, nitride or fluoride anion.

Yet, harvesting reversible multielectron capacity from multivalent systems presents many challenges due to intrinsic material limitations arising from (i) extremely poor electronic conductivity, (ii) poor transport and interfacial charge transfer kinetics and (iii) structural instability during multielectron charge transfer [36–39]. A combination of these factors leads to rapid capacity loss and significant hysteresis during charge–discharge cycles. A large hysteresis implies a poor round trip energy efficiency that makes conversion-based electrodes impractical for most applications. The origin of such large hysteresis in multivalent systems is related to various overpotentials, which originate from charge transfer (electronic or ionic), ohmic, or concentration-driven effects [36–39]. For example, in the case of iron fluorides, a major part of the hysteresis can originate from the intrinsically slow diffusion of Fe vs. Li during the reconversion process that can also favour the formation of intermediate phases that are kinetically driven. In addition, iron fluorides (FeF_3 and FeF_2) are highly ionic solids and therefore extremely insulating in nature [36,37,41]. These and other factors limit the use of iron fluorides for high-capacity batteries despite their very high theoretical specific capacity of 712 mAh g^{-1} which is based on the transfer of three moles of lithium per mole of Fe. There have been numerous reports in literature directed towards improving the charge transfer kinetics and transport by reducing the particle size, optimizing their morphology (or both) and enhancing the local electronic conductivity by carbon coating or the addition of highly conducting diluents such as multilayer graphenes (MLG) or conductive carbon. However, to date, such improvements have not been sufficient for practical use for rechargeable battery applications [42,43].

Recently, our group has investigated the role of electrode architecture on the capacity retention and hysteresis of iron (II and III) fluoride compounds and compared their performance with electrodes fabricated using conventional slurry-based approach having similar sized iron fluoride particles [42]. The latter approach does not involve any kind of electrode architecture. The electrode architecture process described in this work has the following unique features: (i) individual nanosized iron fluoride particles (25–50 nm size) are coated or locally surrounded with MLG to enhance their local electronic conductivity. We refer them as FeF_3–MLG (or FeF_2–MLG), (ii) FeF_3–MLG-coated particles are bound

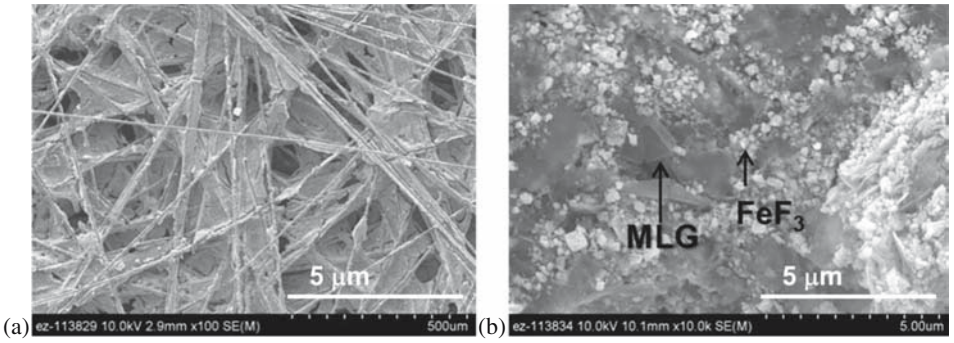

Figure 7. SEM and STEM images showing typical shapes and sizes of FeF_2 and FeF_3 particles and electrodes. (**a**) Pristine FeF_3/FeF_2–MLG carbon fibre electrode, (**b**) FeF_3 and MLG after electrode fabrication at 450°C.

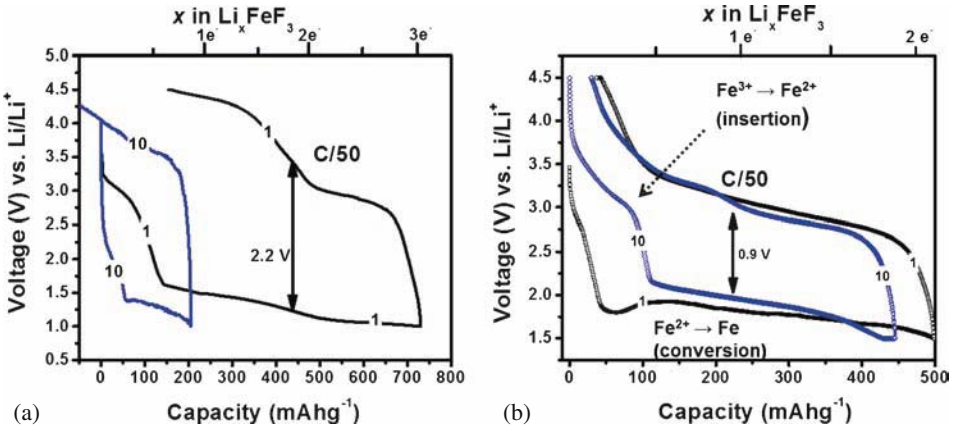

Figure 8. Voltage vs. capacity profiles of Li/FeF_3 cell on (**a**) FeF_3 slurry coated on Al foil, (**b**) FeF_3 supported on carbon fibre electrodes cycled between 1 V/1.5 V and 4.5 V ($C/50$ rate) at 25°C.

to an electronic backbone or current collector comprising an interconnected network of carbon fibres having diameters typically ranging between 5 and 9 μm (figure 7a). This is made possible by using a mesophase pitch carbon (petroleum pitch: p-pitch) as the conductive binder between FeF_3–MLG and carbon fibres as shown in figure 7b.

Our published results demonstrated that the carbon fibre-pitch based electrode architecture produces a significant reduction of hysteresis between the charge and the discharge, from ~2 V (figure 8a) for the conventional slurry-based iron fluoride electrode, to about 0.9 V for the carbon fibre-based matrix (figure 8b) [42]. This also enabled reversible capacity utilization of >450 mAh g^{-1} for FeF_3 with stable cycling (>30 cycles at 25°C) (figure 8b). Furthermore, cycling at elevated temperature (at 60°C, results not shown here), improved the reaction and/or transport kinetics yielding almost theoretical specific capacity (700 mAh g^{-1}) with a good cycle life and additional reduction in the hysteresis.

5. Conclusion

In this article, we have provided a brief review of the current progress in the area of lithium-ion battery materials and showed through various cathode chemistries the role of nanoscale effects towards optimizing the electrode materials for better electrochemical capacity retention and cycle life. Nanosizing of the electrode materials as well as nanocoating the electrode particle surfaces play major roles in improving the electrochemical performance. Electrode architecture at the nanoscale can also facilitate electrochemical transport and capacity utilization. Current research efforts in the area of electrochemical energy storage are directed towards beyond-Li-ion chemistries such as Mg ion, metal–air and Li–sulphur and all solid-state batteries [44–46]. However, fundamental breakthroughs are needed to overcome some of the scientific challenges associated with such high-capacity lithium-ion battery chemistries.

Acknowledgements

This work is supported by the Assistant Secretary for Energy Efficiency and Renewable Energy, Office of Vehicle Technologies of the U.S. Department of Energy. RK acknowledges the support by TN-SCORE grant NSF-EPS-1004083.

References

[1] M S Whittingham, *Chem. Rev*. **104**, 4271 (2004)
[2] A K Shukla, V G Kumar and M K Ravikumar, *Electrochemically enabled sustainability: Devices, materials and mechanisms for energy conversion* edited by Kwong-Yu Chan, Chin-Ying Vanessa Li (CRC Press, 2014) p. 256
[3] M S Whittingham, *Prog. Solid State Chem.* **12**, 41 (1978)
[4] K Mizushima, P C Jones, P J Wiseman and J B Goodenough, *Mater. Res. Bull.* **15**, 783 (1980)
[5] S K Martha, H Sclar, Z S Framowitz, D Kovacheva, N Saliyski, Y Gofer, P Sharon, E Golik, B Markovsky and D Aurbach, *J. Power Sources* **189**, 248 (2009)
[6] S Martha, E Markevich, V Burgel, G Salitra, E Zinigrad, B Markovsky, H Sclar, Z Pramovich, O Heik and D Aurbach, *J. Power Sources* **189**, 288 (2009)
[7] M Sathiya, G Rousse, K Ramesha, C Laisa, H Vezin, M T Sougrati, M-L Doublet, D Foix, D Gonbeau and W Walker, *Nat. Mater.* **12**, 827 (2013)
[8] A K Shukla and T P Kumar, *J. Phys. Chem. Lett.* **4**, 551 (2013)
[9] M M Thackeray, C S Johnson, J T Vaughey, N Li and S A Hackney, *J. Mater. Chem.* **15**, 2257 (2005)
[10] S K Martha, J Nanda, G M Veith and N J Dudney, *J. Power Sources* **199**, 220 (2012)
[11] M M Thackeray, S-H Kang, C S Johnson, J T Vaughey, R Benedek and S Hackney, *J. Mater. Chem.* **17**, 3112 (2007)
[12] M Sathiya, A M Abakumov, D Foix, G Rousse, K Ramesha, M Saubanère, M Doublet, H Vezin, C Laisa and A Prakash, *Nat. Mater.* (2014)
[13] S K Martha, J Nanda, Y Kim, R R Unocic, S Pannala and N J Dudney, *J. Mater. Chem. A* **1**, 5587 (2013)
[14] S K Martha, J Nanda, G M Veith and N J Dudney, *J. Power Sources* **216**, 179 (2012)
[15] T R Penki, S Sekharappa, M Minakshi and N Munichandraiah, Meeting Abstracts, *Electrochem. Soc.*, 81–81 (2014)
[16] K Shiva, H R Matte, H Rajendra, A J Bhattacharyya and C Rao, *Nano Energy* **2**, 787 (2013)
[17] K Shiva, H Rajendra, K Subrahmanyam, A J Bhattacharyya and C Rao, *Chemistry-A Eur. J.* **18**, 4489 (2012)
[18] M K Jana, H Rajendra, A J Bhattacharyya and K Biswas, *Cryst. Eng. Comm.* **16**, 3994 (2014)
[19] W-J Zhang, *J. Power Sources* **196**, 13 (2011)
[20] H Zhou, J Nanda, S K Martha, R R Unocic, I I I H M Meyer, Y Sahoo, P Miskiewicz and T F Albrecht, *ACS Appl. Mater. Interfaces* **6**, 7607 (2014)
[21] J Qu, H Li, J J Henry, S K Martha, N J Dudney, H Xu, M Chi, M J Lance, S M Mahurin and T M Besmann, *J. Power Sources* **198**, 312 (2012)
[22] P Ragupathy, H Vasan and N Munichandraiah, *J. Nano Energy Power Res.* **2**, 139 (2013)
[23] C K Chan, H Peng, G Liu, K McIlwrath, X F Zhang, R A Huggins and Y Cui, *Nat. Nanotech.* **3**, 31 (2008)
[24] Q Wang, P Ping, X Zhao, G Chu, J Sun and C Chen, *J. Power Sources* **208**, 210 (2012)
[25] D Doughty and E P Roth, *Electrochem. Soc. Interface* **21**, 37 (2012)
[26] K Xu, *Chem. Rev*. **114**, 11503 (2014)
[27] G A Nazri and G Pistoia, *Lithium batteries: Science and Technology* (Springer, 2008)

[28] J Wang and X Sun, *Energy Environ. Sci.* **5**, 5163 (2012)
[29] S K Martha, J Grinblat, O Haik, E Zinigrad, T Drezen, J H Miners, I Exnar, A Kay, B Markovsky and D Aurbach, *Angew. Chem. Int. Edn.* **48**, 8559 (2009)
[30] C Johnson, J Kim, C Lefief, N Li, J Vaughey and M Thackeray, *Electrochem. Commun.* **6**, 1085 (2004)
[31] N Yabuuchi, K Yoshii, S-T Myung, I Nakai and S Komaba, *J. Am. Chem. Soc.* **133**, 4404 (2011)
[32] A R Armstrong, M Holzapfel, P Novak, C S Johnson, S H Kang, M M Thackeray and P G Bruce, *J. Am. Chem. Soc.* **128**, 8694 (2006)
[33] J Li, N J Dudney, J Nanda and C Liang, *ACS Appl. Mater. Interfaces* **6**, 10083 (2014)
[34] Y Kim, G M Veith, J Nanda, R R Unocic, M Chi and N J Dudney, *Electrochim. Acta* **56**, 6573 (2011)
[35] F Yang, Y Liu, S K Martha, Z Wu, J C Andrews, G E Ice, P Pianetta and J Nanda, *Nano Lett.* **14**, 4334 (2014)
[36] J Cabana, L Monconduit, D Larcher and M R Palacin, *Adv. Mater.* **22**, E170 (2010)
[37] F Wang, R Robert, N A Chernova, N Pereira, F Omenya, F Badway, X Hua, M Ruotolo, R Zhang and L Wu, *J. Am. Chem. Soc.* **133**, 18828 (2011)
[38] M R Palacin, *Chem. Soc. Rev.* **38**, 2565 (2009)
[39] H Li, P Balaya and J Maier, *J. Electrochem. Soc.* **151**, A1878 (2004)
[40] H Zhou, J Nanda, S K Martha, J Adcock, J C Idrobo, L Baggetto, G M Veith, S Dai, S Pannala and N J Dudney, *J. Phys. Chem. Lett.* **4**, 3798 (2013)
[41] P Liu, J J Vajo, J S Wang, W Li and J Liu, *J. Phys. Chem. C* **116**, 6467 (2012)
[42] S K Martha, J Nanda, H Zhou, J C Idrobo, N J Dudney, S Pannala, S Dai, J Wang and P V Braun, *RSC Adv*. **4**, 6730 (2014)
[43] T Li, L Li, Y L Cao, X P Ai and H X Yang, *J. Phys. Chem. C* **114**, 3190 (2010)
[44] J F Oudenhoven, L Baggetto and P H Notten, *Adv. Energy Mater.* **1**, 10 (2011)
[45] P G Bruce, S A Freunberger, L J Hardwick and J-M Tarascon, *Nat. Mater.* **11**, 19 (2012)
[46] H D Yoo, I Shterenberg, Y Gofer, G Gershinsky, N Pour and D Aurbach, *Energy Environ. Sci.* **6**, 2265 (2013)